

# Statistical and machine learning methods for evaluating trends in air quality under changing meteorological conditions

Minghao Qiu<sup>1,\*</sup>, Corwin Zigler<sup>2</sup>, and Noelle Selin<sup>1,3</sup>

<sup>1</sup>Institute for Data, Systems, and Society, Massachusetts Institute of Technology, Cambridge, USA

<sup>2</sup>Departments of Statistics and Data Science, University of Texas, Austin, USA

<sup>3</sup>Department of Earth, Atmospheric, and Planetary Sciences, Massachusetts Institute of Technology, Cambridge, USA

\*Current address: Department of Earth System Science, Stanford University, USA

**Correspondence:** Minghao Qiu (mhqiu@stanford.edu)

1 **Abstract.** Evaluating the influence of anthropogenic emissions changes on air quality requires accounting for the influence of  
2 meteorological variability. Statistical methods such as multiple linear regression (MLR) models with basic meteorological vari-  
3 ables are often used to remove meteorological variability and estimate trends in measured pollutant concentrations attributable  
4 to emissions changes. However, the ability of these widely-used statistical approaches to correct for meteorological variability  
5 remains unknown, limiting their usefulness in the real-world policy evaluations. Here, we quantify the performance of MLR  
6 and other quantitative methods using simulations from a chemical transport model, GEOS-Chem, as a synthetic dataset. Focus-  
7 ing on the impacts of anthropogenic emissions changes in the US (2011 to 2017) and China (2013 to 2017) on PM<sub>2.5</sub> and O<sub>3</sub>,  
8 we show that widely-used regression methods do not perform well in correcting for meteorological variability and identifying  
9 long-term trends in ambient pollution related to changes in emissions. The estimation errors, characterized as the differences  
10 between meteorology-corrected trends and emission-driven trends under constant meteorology scenarios, can be reduced by  
11 30%-42% using a random forest model that incorporates both local and regional scale meteorological features. We further  
12 design a correction method based on GEOS-Chem simulations with constant emission input and quantify the degree to which  
13 anthropogenic emissions and meteorological influences are inseparable, due to their process-based interactions. We conclude  
14 by providing recommendations for evaluating the impacts of anthropogenic emissions changes on air quality using statistical  
15 approaches.

## 16 1 Introduction

17 Researchers and policy makers have long been interested in understanding the anthropogenic drivers of trends in observed air  
18 pollutant concentrations in order to inform air quality policies. Declining trends in pollutant concentrations such as particu-  
19 late matter with diameter less than 2.5 microns ( $PM_{2.5}$ ) have been observed in many countries that adopted policies to limit  
20 anthropogenic emissions such as  $SO_2$  and  $NO_x$ , including the US (McClure and Jaffe, 2018) and China (Zhang et al., 2019).  
21 As the information on anthropogenic emissions is often unavailable or very uncertain, researchers and policy makers often  
22 rely on the trends in measured air pollutants to assess the effects of policies. Attributing trends in observed concentrations to  
23 anthropogenic emissions changes requires correcting for the influence of changing meteorology, which has become increas-  
24 ingly important but challenging in a changing climate (Saari et al., 2019). Numerous papers attempt to use statistical methods  
25 to separate impacts of meteorology from emissions changes in evaluating trends in air quality, but the performance of these  
26 commonly-used statistical approaches remains unassessed. Further, the impacts of meteorological variability may not even be  
27 distinguishable from air quality trends driven by anthropogenic emission changes, due to their interactions; the magnitude of  
28 this interaction also remains unquantified. In this paper, we devise a model-based experiment for evaluating the performance  
29 of different statistical methods used for meteorological corrections. We focus on a case of identifying emissions-driven linear  
30 trends in measured concentrations of  $PM_{2.5}$  and ozone ( $O_3$ ), when information on the anthropogenic emission is not available.

31 Measured pollutant concentrations are often used as the primary basis for evaluating air quality actions. For example, in  
32 2013, China's central government established targets that aimed to reduce annual average  $PM_{2.5}$  concentrations of three urban  
33 clusters by 15% to 25% between 2012 and 2017 (State Council of the People's Republic of China, 2013). This later translated  
34 into a stringent and binding target of a maximum annual mean  $PM_{2.5}$  concentration of  $60 \mu g/m^3$  in 2017 for Beijing, which  
35 was ultimately reached (the 2017 concentration was  $58.5 \mu g m^{-3}$ ) (Beijing Municipal Ecology and Environment Bureau,  
36 2013). However, several studies estimated that the concentration would have exceeded this target in Beijing were it not for  
37 meteorological conditions in the winter 2017 that favored pollution reductions (Vu et al., 2019; Chen et al., 2019; Cheng  
38 et al., 2019). The European Union and US Environmental Protection Agency (EPA) use a three-year average of the  $PM_{2.5}$   
39 concentration to determine compliance with air quality standards (European Union, 2020; U.S. Environmental Protection  
40 Agency, 2019). The US EPA has also proposed to use statistical approaches that aim to correct for the impacts of weather  
41 variability on  $O_3$  concentrations in the designation processes (Wells et al., 2021).

42 Many studies use multiple linear regression (MLR) models with basic meteorological variables to correct for meteorological  
43 variability in order to estimate the impacts of emissions changes on measured air quality (Otero et al., 2018; Zhai et al., 2019;  
44 Li et al., 2018, 2020; Han et al., 2020; Chen et al., 2020). Zhai et al. (2019) and Li et al. (2020) use MLR models to estimate the

45 degree to which trends in  $PM_{2.5}$  and  $O_3$  from 2013 to 2019 in China were driven by anthropogenic emissions changes. They  
46 first use MLR to predict the  $PM_{2.5}$  and  $O_3$  concentrations with meteorological variables, and then interpret the residuals of  
47 the MLR model as signals resulting from emissions changes. A related approach is to combine MLR with techniques that can  
48 decompose time series of observed concentrations into long-term, seasonal, and short-term components (e.g., Kolmogorov-  
49 Zurbenko (KZ) filters (Zurbenko, 1994)). Ma et al. (2016) and Chen et al. (2019) use KZ filters to calculate the long-term  
50 component of observed  $PM_{2.5}$  and then apply MLR to separate the impacts of long-term meteorological changes on the  
51 concentrations. Henneman et al. (2015) apply MLR to the short-term component (identified by KZ filters) of air pollutant  
52 concentrations near Atlanta during 2000 to 2012, to separate the impact of short-term meteorological variability, and then  
53 estimate the long-term trend in air quality.

54 Other statistical methods including non-linear regression or machine learning models have also been used to correct for  
55 meteorological variability (Holland et al., 1998; Carslaw et al., 2007; Hayn et al., 2009; Vu et al., 2019). One popular method  
56 is to use a generalized additive model (GAM) to estimate non-linear smooth functions of each meteorological variable within a  
57 given smoothing function family with penalization on non-smoothness. The US EPA uses a GAM model of temperature, wind  
58 direction and speed, humidity, pressure, stability, transport trajectories, and synoptic weather to perform weather corrections in  
59 assessing long-term trends in  $O_3$  (Camalier et al., 2007). An increasing number of studies use machine learning models (Grange  
60 et al., 2018; Vu et al., 2019; Zhang et al., 2020; Shi et al., 2021; Qu et al., 2020). Vu et al. (2019) use a random forest model  
61 to predict pollutant concentrations in Beijing with time index and meteorological variables and then calculate the “weather-  
62 normalized” concentration for each day with 1000 sets of meteorological fields drawn from the historical meteorological data.  
63 They found that the decrease of  $PM_{2.5}$  during 2013 to 2017 was largely driven by emissions reductions, although the magnitude  
64 of reduction is smaller when correcting for meteorological variability.

65 Despite a large number of papers that apply various meteorology correction methods, very little is known about whether  
66 these methods can effectively correct for meteorological variability and thus realistically estimate the counterfactual air quality  
67 and reveal the underlying impacts of anthropogenic emissions changes. Most studies cite the prediction performance of their  
68 statistical models (such as  $R^2$  and/or mean squared errors) to justify their method choice and analysis. However, good pre-  
69 diction performance does not guarantee the correct estimation of counterfactuals and causal effects (Runge et al., 2019). The  
70 performance of these meteorology-corrected methods is unable to be assessed using observational data alone, as the underly-  
71 ing emission-driven trends without influence from meteorological variability cannot be derived from data. Further, statistical  
72 analyses often assume that the influence of meteorological variability on pollutant concentration can be cleanly separated from  
73 the influence of anthropogenic emissions changes. This is not completely possible, as the impacts of meteorological variability

74 on pollutant concentration will also vary depending on the emissions. The degree to which this interaction affects the ability to  
75 calculate emissions-related trends under changing meteorology also remains unknown.

76 Here, we conduct a model experiment to evaluate the performance of widely-used statistical models in correcting for me-  
77 teorological variability and estimating emissions-driven trends in air quality (see figure 1). We focus on the impacts of an-  
78 thropogenic emissions changes on annual  $\text{PM}_{2.5}$  and summer  $\text{O}_3$  in the US (2011-2017) and China (2013-2017), two periods  
79 well-studied in previous literature. Using a 3-D atmospheric chemical transport model GEOS-Chem, we simulate two sets of  
80 scenarios – “observational scenarios” with assimilated meteorological inputs (with interannual variability) and “counterfactual  
81 scenarios” with constant meteorological inputs. Using simulated daily concentrations in the observational scenarios, we es-  
82 timate meteorology-corrected trends for each grid cell from regression models using different statistical correction methods.  
83 We then compare the derived trends with the emissions-driven trends in the counterfactual scenarios (which are free of mete-  
84 orological variability by design), calculating the resulting “error” in trend estimation. We further design a correction method  
85 based on GEOS-Chem constant emission simulations, and use it to quantify the degree to which attribution to meteorology and  
86 emissions separately is possible. Finally, we apply the different statistical correction methods to observational data from sur-  
87 face monitoring networks in the US and China, discussing the variability across different methods. We conclude by providing  
88 recommendations for techniques to evaluate air pollution policies under changing meteorological conditions.

## 89 **2 Method**

### 90 **2.1 GEOS-Chem**

91 GEOS-Chem is a global three-dimensional chemical transport model driven by assimilated meteorological data from the God-  
92 dard Earth Observation System (GEOS-5) of the NASA Global Modeling and Assimilation Office (GMAO) (Bey et al. (2001),  
93 <http://www.geos-chem.org/>). The simulation of  $\text{PM}_{2.5}$  in GEOS-Chem represents an external mixture of secondary inorganic  
94 aerosols, carbonaceous aerosols, sea salt, and dust aerosols. GEOS-Chem includes detailed  $\text{O}_3$ - $\text{NO}_x$ -volatile organic carbon  
95 (VOC)-aerosol-halogen tropospheric chemistry (Travis et al., 2016; Sherwen et al., 2016). The GEOS-Chem model has been  
96 previously used to study the changes in  $\text{PM}_{2.5}$  and  $\text{O}_3$  during our studied periods, and model simulations have been shown to  
97 be consistent with the observed concentrations (e.g., see Li et al. (2017a); Xie et al. (2019) for the US, and Li et al. (2018);  
98 Lu et al. (2019); Zhai et al. (2021) for China). Studies in both regions show that the GEOS-Chem model is able to reproduce  
99 the spatial, seasonal, and interannual variability and the long-term trends in observed pollutant concentrations, despite biases  
100 in absolute concentrations in certain species and regions (Heald et al., 2012; Travis et al., 2016; Tian et al., 2021).

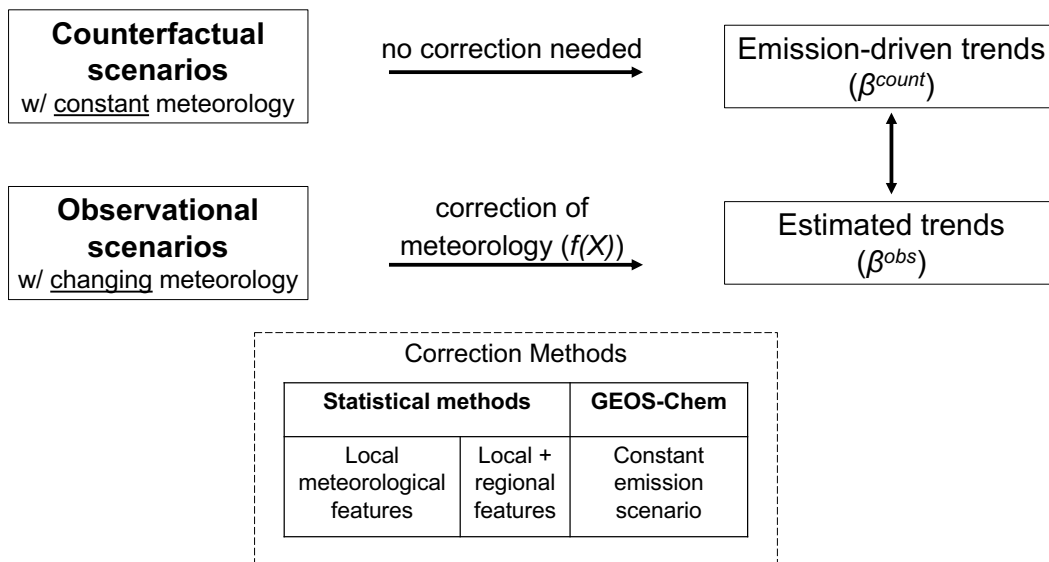


**Figure 1.** Overview of research methodology. Terms and coefficients are linked to the associated terms in equation 1 and table 1.

101 We use GEOS-Chem version 12.3.0 with a horizontal resolution of  $0.5^\circ \times 0.625^\circ$  in North America and Asia (Wang et al.,  
 102 2004). For each scenario, we first conduct a global run at a horizontal resolution of  $4^\circ \times 5^\circ$ , with a 12 month spin-up. These  
 103 global runs are then used as the boundary conditions for nested simulations in the US and China with finer resolution of  
 104  $0.5^\circ \times 0.625^\circ$ .

## 105 2.2 GEOS-Chem scenarios

106 Table 1 shows the simulations included in our model experiments. We simulate two sets of scenarios – “observational scenarios”  
 107 with interannual variability in meteorology and “counterfactual scenarios” with constant meteorological inputs. Both scenarios  
 108 use the same emissions inventory as input (see section 2.3). For each grid cell, we estimate the linear trends in pollutant  
 109 concentrations from simulated daily  $PM_{2.5}$  and  $O_3$  concentrations. We focus on the daily 24-hour average  $PM_{2.5}$  over all  
 110 seasons, and the maximum daily average 8-hour (MDA8)  $O_3$  in summer (June, July, August). Our focus on the three summer  
 111 months is consistent with many previous studies (e.g., Shen et al. (2015)), although this may not capture the peak ozone  
 112 season for certain regions of the US and China. Our GEOS-Chem simulations use meteorological fields from the Modern-  
 113 Era Retrospective analysis for Research and Applications, Version 2 (MERRA-2) (Gelaro et al., 2017). We aggregate the  
 114 hourly meteorological data for consistency with the pollutant concentrations: a 24-hour average for  $PM_{2.5}$  analysis and the  
 115 corresponding 8-hour average for  $O_3$ . Meteorological features that are used in the statistical models can be found in section  
 116 2.4.

### 117 **2.2.1 Observational scenarios**

118 Observational scenarios simulate  $\text{PM}_{2.5}$  and  $\text{O}_3$  under changing emissions and changing meteorological fields. Trends es-  
119 timated under the observational scenarios ( $\beta^{obs}$ ) are subject to the influences of interannual meteorological variability. Our  
120 model experiments were not specifically designed to reproduce observed air quality in these two regions, but rather to pro-  
121 vide a realistic test case to evaluate the performances of statistical methods. Nevertheless, as shown in figure A1 and A2, the  
122 simulated concentrations in  $\text{PM}_{2.5}$  and  $\text{O}_3$  largely reproduce the daily variability in observed pollutant concentrations. The  
123 linear trends in simulated  $\text{PM}_{2.5}$  and  $\text{O}_3$  concentrations in the observational scenario are largely consistent with trends of the  
124 measured concentrations. For example, the average trend ( $\pm$ one standard deviation) in the US is  $-0.27 \pm 0.30 \mu\text{g}^{-3}/\text{year}$  (obser-  
125 vation) and  $-0.39 \pm 0.24 \text{ ppb}/\text{year}$  (GEOS-Chem) for  $\text{PM}_{2.5}$ , and  $-0.91 \pm 0.98 \text{ ppb}/\text{year}$  (observation) and  $-1.02 \pm 0.83 \text{ ppb}/\text{year}$   
126 (GEOS-Chem) for  $\text{O}_3$ . The only exception is that our model cannot reproduce the increasing  $\text{PM}_{2.5}$  trends in the Northwest  
127 US because we do not consider interannual variability in biomass burning emissions.

### 128 **2.2.2 Counterfactual scenarios**

129 Counterfactual scenarios simulate  $\text{PM}_{2.5}$  and  $\text{O}_3$  under changing emissions but constant meteorology. All simulation years in  
130 the counterfactual scenario use the meteorological fields of the start year (2011 for the US, 2013 for China). Trends estimated  
131 under the counterfactual scenario ( $\beta^{count}$ ) are not subject to interannual meteorological variability; we use this as a proxy for  
132 the trends in pollutant concentrations driven by emissions changes alone. In a sensitivity analysis, we also simulate the counter-  
133 factual scenario for China using the meteorological fields at the end year 2017 (at  $4 \times 5$  degree resolution, due to computational  
134 constraints). We find that the linear trend in  $\text{PM}_{2.5}$  and  $\text{O}_3$  for each grid cell is highly consistent in the counterfactual scenarios  
135 across the choice of the meteorological years (see figure A5).

### 136 **2.2.3 Assumptions for GEOS-Chem experiments**

137 It is important to note that we do not assume our GEOS-Chem simulations perfectly represent the underlying pollutant con-  
138 centration in the real world (although the model compares relatively well with the observational data). Rather, our main focus  
139 is to evaluate how much different statistical methods can explain the differences between the observational and counterfactual  
140 scenarios. The assumption here is that the differences between observational and counterfactual scenarios are useful approxima-  
141 tions of the impacts of meteorological variability on pollutant concentrations. The implications of uncertainty in GEOS-Chem  
142 for our results can be found in the discussion section.

<b>GEOS-Chem scenarios</b>	<b>Emissions inventory</b>	<b>Meteorological fields</b>	<b>Trend estimates</b>	<b>Meteorological correction</b>
Counterfactual scenarios	<b>Changing</b> 2011-2017 (US) 2013-2017 (China)	<b>Constant</b> 2011 (US) 2013 (China)	$\beta^{count}$	
Observational scenarios	<b>Changing</b> 2011-2017 (US) 2013-2017 (China)	<b>Changing</b> 2011-2017 (US) 2013-2017 (China)	$\beta^{uncorrected}$  $\beta^{MLR}$  $\beta^{GAM}$  $\beta^{RF}$  $\beta^{LASSO-regional}$  $\beta^{RF-regional}$  $\beta^{gc}$	No correction  Linear combination of local features  GAM using local features  RF using local features  LASSO using local and regional features  RF using local and regional features  Use simulations from constant emissions scenarios
Constant emissions scenarios	<b>Constant</b> 2011 (US) 2013 (China)	<b>Changing</b> 2011-2017 (US) 2013-2017 (China)		

Table 1: Overview of GEOS-Chem scenarios and meteorological correction methods.

## 143 **2.3 Emissions inventory**

144 For the US, we use the National Emissions Inventory 2011 (NEI 2011) as a baseline emissions inventory and scale the emissions  
145 in 2012 to 2017 to match the annual total emissions each year (U.S. Environmental Protection Agency, 2021a). For China,  
146 we use the monthly Multi-resolution Emission Inventory for China (MEIC) during 2013 to 2017 (Li et al., 2017b; Zheng  
147 et al., 2018). During the studied time periods, the US and China experienced dramatic decreases in anthropogenic emissions,  
148 particularly in SO<sub>2</sub> and NO<sub>x</sub>. In the US, total anthropogenic emissions of SO<sub>2</sub> decreased by 57% and NO<sub>x</sub> emissions decreased  
149 by 26% during 2011 to 2017 (see figure A3). In China, anthropogenic SO<sub>2</sub> emissions decreased by 59% and NO<sub>x</sub> emissions  
150 decreased by 21% during the 2013-2017 period (see figure A4).

151 Natural emissions of multiple chemical species are calculated online in the simulations (rather than prescribed) in the GEOS-  
152 Chem model and thus can be influenced by meteorological variability (see Keller et al. (2014) for more details). Impacts of  
153 meteorology on PM<sub>2.5</sub> and O<sub>3</sub> concentrations through changes in the natural emissions are considered here as part of the  
154 meteorology-concentration relationship. These emissions include NO<sub>x</sub> emissions from lightning and soil processes, sea salt  
155 emissions, dust emissions, and biogenic volatile organic carbon (VOC) emissions. However, biomass burning emissions are  
156 prescribed in the GEOS-Chem model and we hold them constant at the level of the start year. We make this simplification  
157 because the GEOS-Chem model uses biomass burning emissions from external inventories such as Global Fire Emissions  
158 Database (Werf et al., 2017), and it is impossible to distinguish natural fire emissions (part of the meteorological variability)  
159 from anthropogenic fire emissions (e.g., from farm residual burning). The role of natural emission changes in the meteorology-  
160 air quality relationship is further expanded on in the discussion section.

## 161 **2.4 Statistical and machine learning models**

### 162 **2.4.1 Model with local meteorological variables**

163 We assess the performance of statistical and machine learning models to correct for the meteorological variability in the  
164 observational scenarios. We evaluate these methods with a commonly-used framework (e.g., used in Li et al. (2018) and  
165 Zhai et al. (2019)) which models the air pollutant concentrations of each individual grid cell using an additive form of a  
166 trend component, a meteorology component, and time fixed effects (to capture daily and monthly variability not related to  
167 meteorology). More specifically, we estimate the following regression equation for each grid cell  $i$ :

$$168 \quad y_{it} = \beta_i^{obs} \times t + f_i(X_{it}) + \eta_{it} + \epsilon_{it} \quad (1)$$



169 where  $y_{it}$  denotes the  $\text{PM}_{2.5}$  or  $\text{O}_3$  concentration at grid cell  $i$  on day  $t$ .  $t$  is the time index (e.g., in the US,  $t=1$  for January 1st,  
170 2011 and  $t=2$  for January 2nd, 2011).  $X_{it}$  denotes the local meteorology features (i.e. meteorological variables in grid cell  $i$  on  
171 day  $t$ ).  $\eta_{it}$  is the month-of-year $\times$ day-of-month fixed effect to capture daily and monthly variability of pollutant concentrations  
172 that are not related to the meteorological variability (e.g., seasonal cycle in  $\text{O}_3$  and  $\text{PM}_{2.5}$ ).  $\epsilon_{it}$  is the normally-distributed error  
173 term.  $\beta_i^{obs}$  represents the meteorology-corrected trend in  $\text{PM}_{2.5}$  or  $\text{O}_3$  concentration for grid cell  $i$  estimated with the standard  
174 ordinary least square method. We use the absolute differences  $|\beta_i^{obs} - \beta_i^{count}|$  to evaluate the performance of different methods  
175 to correct for meteorological variability for any given grid cell  $i$ .

176 Here,  $f_i(X_{it})$  represents the specifications of local meteorological features for grid cell  $i$  under different methods. In addition  
177 to the commonly-used multiple linear regression (MLR) model, we also evaluate the following models with higher flexibility:  
178 polynomial regression models (quadratic, cubic), cubic spline models, generalized additive models (GAM, implemented with R  
179 package “mgcv” by Wood (2011)), and Random Forest (RF) models. We refer to the trend estimates estimated without  $f_i(X_{it})$   
180 as “uncorrected”. We focus on the methods in table 1 in the main manuscript, and the performance of the other methods can  
181 be found in table A1 and A2. Note that the time fixed effects are modeled differently in RF models due to the estimation  
182 procedure. More details on the implementation of RF can be found in SI.

183 We use the following ten variables from MERRA-2 as our selected meteorological features for the statistical analysis: surface  
184 temperature, precipitation, humidity, planetary boundary layer height, cloud fraction, surface air pressure, and wind speed (U  
185 and V direction, at surface and 850 hpa level). These variables are the most commonly used features in previous studies. We also  
186 perform sensitivity analyses that include nine more meteorological features: direct photosynthetically-active radiation, diffuse  
187 photosynthetically-active radiation, tropopause pressure, friction velocity, top soil moisture, root soil moisture, snow depth,  
188 surface albedo, and surface air density. These features are selected because they are used as primary or intermediate inputs  
189 for calculating  $\text{PM}_{2.5}$  or  $\text{O}_3$  concentrations in the GEOS-Chem model and may be relevant for the variability in pollutant  
190 concentrations.

#### 191 **2.4.2 Model with local and regional meteorological variables**

192 We also evaluate models that use both local and regional meteorological features. Regional meteorological features are impor-  
193 tant for explaining variability in local pollutant concentrations due to 1) pollution transport from neighboring locations, and  
194 2) influences from meteorological systems at synoptic scale (i.e. large scale weather systems that span over 1000 kilometers  
195 such as circulation patterns) (Tai et al., 2012; Shen et al., 2015; Zhang et al., 2018; Leung et al., 2018; Han et al., 2020). As  
196 the incorporation of both local and regional features can quickly expand the dimensionality of the feature space, here we use  
197 the Least Absolute Shrinkage and Selection Operator (LASSO) and the Random Forest (RF) model, two statistical models that

198 show good prediction performances with high dimensional data inputs. We estimate the following equations:

$$199 \quad y_{it} = \beta_i^{obs} \times t + g_i(X_{it}, Z_t) + \eta_{it} + \epsilon_{it} \quad (2)$$

200 where  $g_i()$  denotes the functional form fitted by LASSO or RF.  $X_{it}$  again denotes the local meteorology features for grid cell  
201  $i$  on day  $t$ .  $Z_t$  denotes the regional scale meteorology features including the meteorological features for every grid cell in the  
202 US on day  $t$  (98 cells in  $4 \times 5$  degrees; we choose a relatively coarse resolution due to computational cost). Meteorological  
203 information in each location in the US may help explain the pollutant concentrations in grid cell  $i$ . In total, we have 10 local  
204 features ( $X_{it}$ ) and  $10 \times 98 = 980$  regional scale features ( $Z_t$ ). The coefficient  $\beta_i^{obs}$  is obtained with the double machine learning  
205 approach by Chernozhukov et al. (2018). In particular, the hyper-parameters and coefficients of LASSO and RF are selected  
206 and fitted using 4-fold cross-validation to avoid the “overfitting risk”. More details on the implementation of LASSO and RF  
207 can be found in SI.

## 208 **2.5 Correction approach using GEOS-Chem constant emissions scenario**

209 We further design and evaluate an approach to correct for meteorology variability with GEOS-Chem simulations (referred  
210 to as “constant-emis” approach). The “constant-emis” approach uses GEOS-Chem simulations with constant anthropogenic  
211 emissions and changing meteorological fields (“constant emissions scenarios” in table 1). All years in the constant emissions  
212 scenario use anthropogenic emissions of the start year (2011 for the US, 2013 for China). We estimate the following equations:  
213

$$214 \quad y_{it} = \beta_i^{gc} \times t + SIM_{it} + \eta_{it} + \epsilon_{it} \quad (3)$$

215 where  $SIM_{it}$  denotes the simulated concentrations on day  $t$  in grid cell  $i$  in the constant emissions scenarios.  $SIM_{it}$  serves a  
216 similar purpose as the term “ $f_i(X_{it})$ ” in equation 1, but comes from the GEOS-Chem simulation. Some previous studies have  
217 also used model simulations with constant emissions input as a way to characterize meteorological variability (Zhong et al.,  
218 2018; Zhao et al., 2020).  $\beta_i^{gc}$  is the estimated meteorology-corrected trend in  $PM_{2.5}$  or  $O_3$  concentration using this model-based  
219 correction method.

220 Compared to previous statistical and machine learning approaches, the “constant-emis” approach better captures the meteo-  
221 rological variability as simulated in GEOS-Chem (as  $SIM_{it}$  are directly taken from GEOS-Chem). Therefore, the difference  
222 between the trend estimates ( $\beta^{gc}$ ) and counterfactual trends ( $\beta^{count}$ ) provides a conceptual minimum for estimation errors us-

223 ing the framework of equation 1 to perform meteorological corrections. The commonly-used framework of equation 1 assumes  
224 that the impacts of meteorology variability can be separated from the impacts of anthropogenic emissions. In our experiments,  
225 this assumption indicates that the differences between the counterfactual scenario and the observational scenario can be solely  
226 explained by the meteorological variables. However, the difference in pollutant concentrations between these scenarios is also  
227 in part driven by emissions in their interaction with meteorology (despite the fact that our different scenarios use the same  
228 emissions inventory). We use  $|\beta_i^{gc} - \beta_i^{count}|$  to quantify the estimation error associated with ignoring such interactions in this  
229 framework.

## 230 **2.6 Air quality observation data**

231 We use the surface air quality measurements from the Air Quality Systems administered by the US EPA (U.S. Environmental  
232 Protection Agency, 2021b). We use the daily 24-hour average of  $PM_{2.5}$  concentrations for all months and the daily maximum  
233 8-hour average (MDA8)  $O_3$  concentrations for June, July, and August. Figure A1 shows the locations, trends in measured  
234 concentrations, and correlations between GEOS-Chem simulations and measured concentrations.

235 The surface air quality measurements in China are derived from the monitoring network administered by the China's Ministry  
236 of Ecology and Environment (2021). The monitoring network was launched in 2013 and has expanded to all prefecture-level  
237 cities in mainland China. We use the daily 24-hour average of  $PM_{2.5}$  concentrations and the MDA8  $O_3$  concentrations for  
238 summer. Figure A2 shows the locations, trends in measured concentrations, and correlations between GEOS-Chem simulations  
239 and measured concentrations.

240 We use the meteorological variables from MERRA-2 when performing meteorology corrections at these monitoring stations,  
241 because the meteorology information is not available for all these variables at the station level. This is consistent with previous  
242 analyses estimating the meteorology-corrected trends using observational air quality data (e.g., Li et al. (2018)).

## 243 **3 Results**

### 244 **3.1 Performance of different correction methods: US (2011-2017)**

245 Figure 2A and 2C show the trends in  $PM_{2.5}$  and  $O_3$  concentrations in the counterfactual scenarios in the US. When holding  
246 meteorological fields constant across years, decreasing trends in the simulated  $PM_{2.5}$  concentrations across the US result from  
247 decreasing anthropogenic emissions. The counterfactual scenario also shows negative linear trends in  $O_3$  concentrations in all  
248 but three grid cells in the West. Increases in summer  $O_3$  in these locations result from the non-linear relationship between  $O_3$   
249 concentrations and  $NO_x$  emissions.

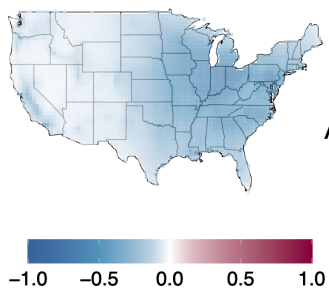
250 Figure 2B and 2D show the degree to which different meteorological correction methods can recover the emissions-driven  
251 trends in the counterfactual scenarios. When no correction for meteorology is performed (“uncorrected” in figure 2B), we  
252 observe large estimation errors in trend estimates over the Northeast and Southern US by up to  $0.25 \mu\text{g m}^{-3}/\text{year}$ , an error  
253 that is 50% of the counterfactual trends. We find that the widely-used MLR method does not help reduce these errors in  $\text{PM}_{2.5}$   
254 trend attributions. MLR has a modest impact on reducing the errors in Northeast US, but it does not decrease the errors over  
255 the Southern US and leads to even higher errors over Midwest. Nationwide, the average magnitude of errors (relative to the  
256 counterfactual scenario) *increases* with the MLR correction ( $0.083 \mu\text{g m}^{-3}/\text{year}$ ) compared to the uncorrected case ( $0.066 \mu\text{g}$   
257  $\text{m}^{-3}/\text{year}$ ). Among the five methods, we find that the RF model using both local and regional scale features (“RF-regional” in  
258 figure 2) offers the best performance in recovering the trends in the counterfactual scenarios and is the only method that yields  
259 smaller errors than the uncorrected case (the nationwide average error decreased by  $0.019 \mu\text{g m}^{-3}/\text{year}$ , or 28% less). The  
260 RF-regional model also outperforms the RF-local and LASSO-regional models, suggesting the importance of considering non-  
261 linearity, interactions between different meteorological features, and regional meteorology information in correctly adjusting  
262 for the impacts of meteorology.

263 Meteorological variability also has a substantial influence on the summertime  $\text{O}_3$  trends in the US during this period (as  
264 shown in figure 2D). Relative to the counterfactual scenario, the uncorrected  $\text{O}_3$  trends are biased by over 1-2 ppb/year in large  
265 areas of California, Midwest and Southern US (as much as 320% of the counterfactual trends). This is largely driven by the fact  
266 that the 2011 and 2012 summer was particularly hot in these regions and led to higher concentrations of  $\text{O}_3$  at the beginning of  
267 this 7-year period (see figure A7 for the Southern and Midwest US). Therefore, failure to correct for meteorological variability  
268 results in much more negative trend estimates in the  $\text{O}_3$  concentrations in these areas compared to the counterfactual scenario  
269 (see figure A6). Meteorology corrections with MLR or GAM help reduce these estimation errors substantially (nationwide  
270 average error is reduced by 51% using MLR or 57% using GAM compared to uncorrected trends), while large errors still  
271 persist in the Midwest and South. Similar to the case of  $\text{PM}_{2.5}$ , the RF-regional model offers the best performance in correcting  
272 for meteorological variability (the national average error is further reduced by 42%, compared to MLR), and it is especially  
273 helpful in reducing the errors over the Midwest and South (regional average error is reduced by 64% and 44%, respectively,  
274 compared to MLR).

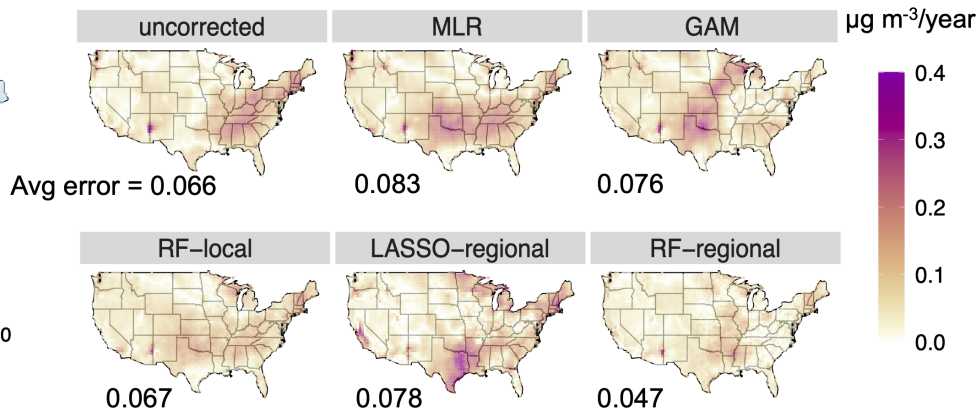
### 275 3.2 Performance of different correction methods: China (2013-2017)

276 Figure 3A and 3C show the trends in  $\text{PM}_{2.5}$  and  $\text{O}_3$  concentrations in the counterfactual scenarios in China. We find a sub-  
277 stantial decline in simulated  $\text{PM}_{2.5}$  concentration during 2013 to 2017, particularly in eastern and central China. In contrast,  
278 there is little change in the simulated  $\text{PM}_{2.5}$  concentrations in western China in the counterfactual scenario, where  $\text{PM}_{2.5}$  is

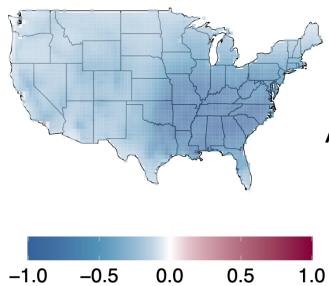
### A Counterfactual $PM_{2.5}$ trends



### B Absolute errors in $PM_{2.5}$ trend estimates



### C Counterfactual $O_3$ trends



### D Absolute errors in $O_3$ trend estimates

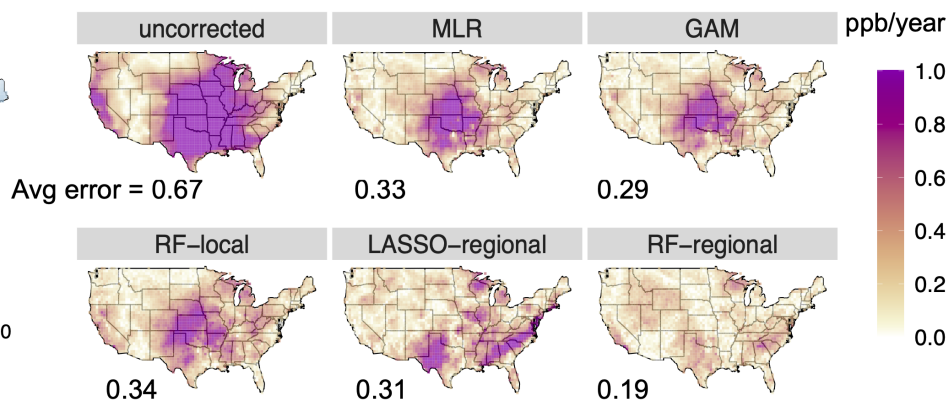


**Figure 2.** Trend estimates of daily annual  $PM_{2.5}$  (Panels A and B) and summer  $O_3$  (C and D) in the US. Panels A and C show trend estimates under the counterfactual scenario ( $\beta^{count}$ ). Panels B and D show the absolute magnitude of errors of trend estimates under different correction methods compared with the counterfactual scenarios ( $|\beta^{obs} - \beta^{count}|$ ). The average of the absolute errors for each method is shown in the figure. Unit of trend estimate is  $\mu\text{g m}^{-3}/\text{year}$  for  $PM_{2.5}$  or  $\text{ppb}/\text{year}$  for  $O_3$ .

279 dominated by dust species largely driven by natural processes (see figure A9). For summer O<sub>3</sub>, there are decreasing trends in  
280 the counterfactual scenario in most parts of China, except for North China and some urban areas. This is largely consistent with  
281 previous studies that attempt to attribute emissions-related changes in O<sub>3</sub> concentrations during this period based on modeling  
282 or observational data (Li et al., 2018, 2020; Lu et al., 2020).

283 Figure 3B shows the magnitude of estimation errors in the trend estimates of annual PM<sub>2.5</sub> in China under different correction  
284 methods. We find the underlying meteorological variability has a substantial impact on PM<sub>2.5</sub> trends in China during this  
285 period. We observe large differences between the uncorrected and counterfactual trends in simulated PM<sub>2.5</sub> concentrations,  
286 particularly in Northwest and Northeast China. Similar to the model experiments in the US, we find that MLR and GAM  
287 methods fail to correct for this underlying meteorological variability and lead to further increases in estimation errors in many  
288 locations. Relative to the counterfactual scenario, the nationwide average error increases to 0.90 μg m<sup>-3</sup>/year with MLR  
289 and 1.06 μg m<sup>-3</sup>/year with GAM (compared to 0.89 μg m<sup>-3</sup>/year with no correction). We find that the RF-regional model  
290 recovers the counterfactual trends better than other methods (nationwide average error: 0.64 μg m<sup>-3</sup>/year; an improvement by  
291 30% relative to MLR), but it is still not able to correct for the persistent estimation errors over Northwest China. We further  
292 analyze the performance of correction methods for the different component species of PM<sub>2.5</sub>. As shown in figure A10 and  
293 A11, the MLR model is particularly unable to correct for the impacts of meteorological variability on nitrate and dust species.  
294 Compared with MLR, the RF-regional model better corrects for the impacts of meteorology on secondary organic aerosol  
295 species in South and Central China and ammonium in Northeast, but only yields modest improvement in correcting for the  
296 errors in dust concentrations over Northwest China (see figure A12). In a sensitivity analysis, we use an approach that first fits  
297 RF-regional models of each individual PM<sub>2.5</sub> species, and then combines predictions for each species to derive trend estimates.  
298 The results are largely similar to the main approach that directly fits the total PM<sub>2.5</sub> concentration (see figure A13).

299 Figure 3D shows the magnitude of errors in the trend estimates for summer O<sub>3</sub> under different correction methods in  
300 China. We find that the MLR model only modestly reduces the estimation errors compared to the uncorrected cases, and the  
301 RF-regional model offers the best overall performance. The nationwide average error is reduced to 0.28 ppb/year using the RF-  
302 regional model (relative to 0.43 ppb/year uncorrected and 0.41 ppb/year with MLR). Similar to the evaluation of summer time  
303 O<sub>3</sub> in the US, we find the non-linear models (GAM, RF-local) perform better than MLR, but are not as good as the RF-regional  
304 model. Surprisingly, the LASSO-regional model performs the worst in recovering the counterfactual trends. Compared to the  
305 US case, we find that the impacts of meteorological variability on O<sub>3</sub> and the method performances are much more spatially  
306 heterogeneous (see figure A6, A8), which may be partially due to the more heterogeneous O<sub>3</sub> regimes in China during this  
307 period.

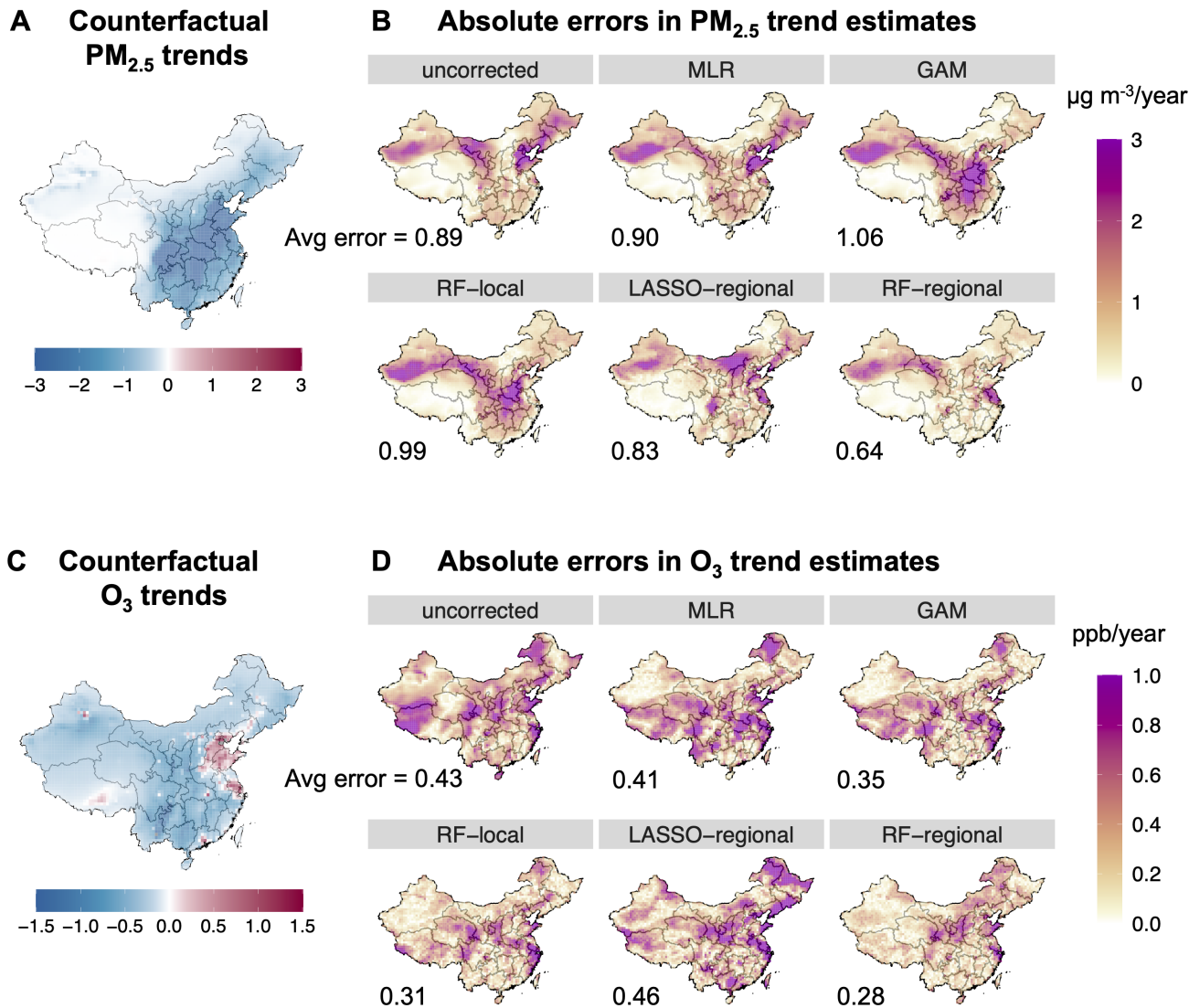


**Figure 3.** Trend estimates of daily annual  $PM_{2.5}$  (Panels A and B) and summer  $O_3$  (C and D) in China. Panels A and C show trend estimates under the counterfactual scenario ( $\beta^{count}$ ). Panels B and D show the absolute magnitude of errors of trend estimates under different correction methods compared with the counterfactual scenarios ( $|\beta^{obs} - \beta^{count}|$ ). The average of the absolute errors for each method is shown in the figure. The unit of the trend estimate is  $\mu\text{g m}^{-3}/\text{year}$  for  $PM_{2.5}$  or ppb/year for  $O_3$ .

### 308 **3.3 Limitations in separating meteorological and emissions influence: quantified with constant emission scenarios**

309 In our model experiments in both US and China, we find large differences remain between the trends evaluated with statistical  
310 models (even the best-performing RF-regional model) and counterfactual trends. The remaining differences could result from  
311 two different factors: 1) the statistical model cannot capture the complex relationship between meteorology and pollutant  
312 concentrations, and/or 2) the differences between the observational scenarios and counterfactual scenarios depend not only  
313 on the meteorological variability but also the anthropogenic emissions in their interaction with meteorology (i.e. impacts of  
314 meteorology on air quality also depend on the level of emissions).

315 We quantify the potential magnitude of this second factor using our constant-emis approach. As the constant-emis approach  
316 captures the exact relationship between meteorology and pollutant concentrations in GEOS-Chem, the error of the constant-  
317 emis approach is only associated with the second factor above and thus provides a conceptual minimum of the estimation errors  
318 that can be achievable by any statistical approach. Figure 4 shows the estimation errors of trend estimates using the constant  
319 emissions scenarios simulated by GEOS-Chem. We focus on the trends in summer O<sub>3</sub> in the US and annual PM<sub>2.5</sub> in China, for  
320 which we see the largest impacts of meteorological variability on the pollutant trends and the largest improvements in reducing  
321 estimation errors from the correction methods. Compared to the statistical models (e.g., MLR and RF-regional in figure 4A  
322 and 4C), trends evaluated using the constant-emis approach are very similar to the trends in the counterfactual scenarios. The  
323 national average error of trend estimates is only 0.04 ppb/year for the O<sub>3</sub> trends in the US (relative to 0.33 ppb/year under MLR  
324 or 0.19 ppb/year under RF-regional), and only 0.08 μg m<sup>-3</sup>/year for the PM<sub>2.5</sub> trends in China (relative to 0.91 μg m<sup>-3</sup>/year  
325 under MLR or 0.64 μg m<sup>-3</sup>/year under RF-regional).

326 However, the estimation errors calculated above are still non-negligible and can be large in certain regions. As shown in Fig-  
327 ure 4B and 4D, the constant-emis approach generally yields trend estimates biased by 10% relative to the counterfactual trends,  
328 but the errors can be up to 40% in certain areas. This error term is the result of ignoring how emissions could potentially influ-  
329 ence the impacts of meteorology on the pollutant concentrations – that is, the impacts of the same meteorological variability  
330 on concentrations may be different in the start year (with high emissions) compared to the end year (with low emissions).

### 331 **3.4 Application to observational data**

332 Figure 5 shows the regional trends in O<sub>3</sub> in the US and trends in PM<sub>2.5</sub> in China estimated from the observational data from  
333 surface monitoring networks and the GEOS-Chem simulations (only grid cells that overlap with monitor locations are shown  
334 here). Here, to correct for the meteorology variability in observational data, we implement the same set of statistical methods as  
335 shown in Table 1, but with different numerical coefficients directly derived from the observational data. When applying different



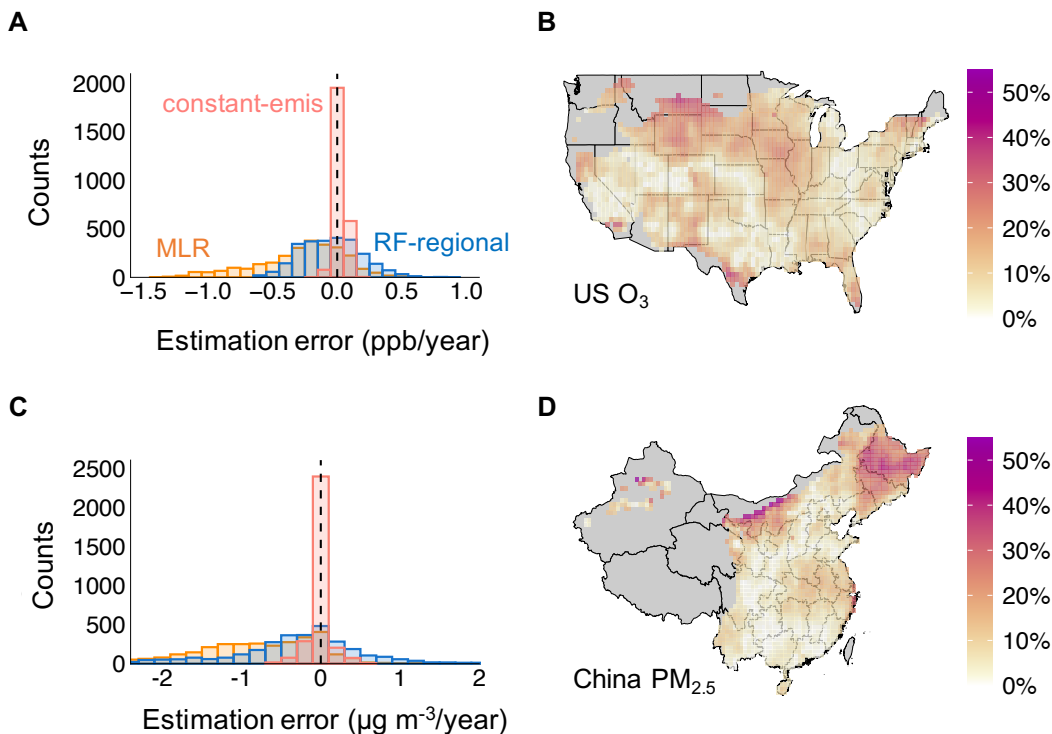


**Figure 4.** Panels A and C show the histogram of estimation errors in trend estimates assessed using MLR, RF-regional and constant-emis. Panels B and D show the errors assessed with the constant-emis method as a percentage of the trends in the counterfactual scenario ( $|\beta^{gc} - \beta^{count}|/|\beta^{count}|$ ). Panels B and D only show grid cells with a trend in the counterfactual scenarios  $>0.2$  ppb/year or  $>0.2 \mu\text{g m}^{-3}$ /year; remaining grid cells are shown in gray. Panels A and B illustrate the summer O<sub>3</sub> trends in the US. Panels C and D illustrate the annual PM<sub>2.5</sub> trends in China.

336 meteorological correction methods to the observational data, our analysis reveals that the choice of methods for meteorological  
 337 correction can yield very different results for certain regions. For example, the regional average uncorrected O<sub>3</sub> trend is -1.49  
 338 ppb/year and -1.15 ppb/year in Midwest and Southern US, respectively, which overestimates the reductions in concentrations  
 339 attributable to anthropogenic emissions changes (figure 5A). Correcting for the meteorological variability with MLR model  
 340 yields a regional average trend at -0.54 ppb/year in Midwest (a decrease by 53% in magnitude relative to uncorrected trends)  
 341 and -0.71 ppb/year in the Southern US (a decrease by 52%). RF-regional model further reduces the absolute magnitude of  
 342 the declines in O<sub>3</sub> attributable to emissions reductions to -0.02 ppb/year for Midwest and -0.40 ppb/year for the Southern  
 343 US. Importantly, these patterns are consistent with the results from our model experiments in these regions: the RF-regional  
 344 model also estimates a much less negative emissions-driven trend in the Southern US compared to the uncorrected case and  
 345 MLR estimates in the GEOS-Chem simulations. For the GEOS-Chem simulations, RF-regional estimates are 39% smaller than

346 MLR estimates, and this is comparable to the magnitude changes for the observational data (RF-regional estimates are 44%  
 347 smaller than MLR). As the RF-regional model outperforms the other correction methods in recovering counterfactual trends in  
 348 the GEOS-Chem simulations, this potentially also suggests a better performance of RF-regional in recovering the underlying  
 349 emission-driven trends when applying to the observational data.

350 We find similar consistency in the method performances between observational data and GEOS-Chem simulations in China  
 351 as well (figure 5B). When applying to the observational data from the surface monitoring network, a much smaller reduction  
 352 of  $PM_{2.5}$  concentrations is attributed to anthropogenic emissions changes in the North, Northeast and East of China using  
 353 the RF-regional model, relative to the MLR estimates. For example, the average emissions-driven trend estimated from the  
 354 observational data is  $-4.9 \mu g m^{-3}/year$  in Beijing under the RF-regional model, compared with  $-9.6 \mu g m^{-3}/year$  under the  
 355 MLR model. These patterns are consistent with the patterns of the trend estimates estimated from our GEOS-Chem simulations  
 356 with different statistical methods.

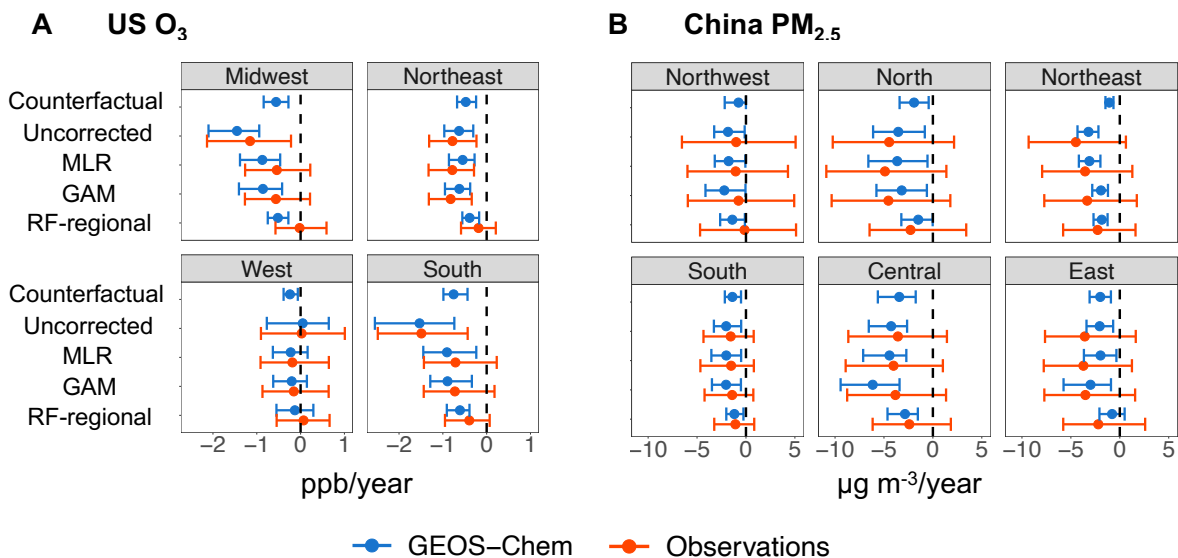


**Figure 5.** Trends in  $O_3$  in the US (panel A) and  $PM_{2.5}$  in China (panel B) estimated from the observational data (red) and GEOS-Chem simulations (blue) under different correction methods. Trends in pollutant concentrations are estimated at the monitor level (for the observational data) or at the grid cell level (for GEOS-Chem simulations). The point indicates the average value of the assessed trends of all monitors (or grid cells) within a region. The error bars show the 10th and 90th percentile of the assessed trends of all monitors/grid cells within a region. Panel A illustrates the summer  $O_3$  trends in the US (unit: ppb/year). Panel B illustrates the annual  $PM_{2.5}$  trends in China (unit:  $\mu g/m^3/year$ ). We classify the US states into four regions according to the US Census Bureau and classify China's provinces into six regions based on the structure of China's subnational electric grid. Observational data are derived from U.S. Environmental Protection Agency (2021b) and China's Ministry of Ecology and Environment (2021).

## 357 4 Discussion

358 We designed a model experiment that enables us to directly quantify the performance of different statistical models to evaluate  
359 the trends in pollutant concentrations driven by anthropogenic emissions changes. Based on our evaluations of either  $PM_{2.5}$   
360 or  $O_3$  trends across the US and China during periods of recent emission declines, our analysis shows that widely-used MLR  
361 and GAM methods do not perform well in correcting for the meteorological variability and recovering simulated emissions-  
362 driven trends. We propose a random forest model that uses both local and regional meteorological features, which offers the  
363 best overall performance in recovering the emissions-driven trends across both species and countries. Applying this model to  
364 observational data suggests that estimates based on MLR or similar methods may overestimate the impacts of anthropogenic  
365 emissions changes on the decline of pollutant concentrations in certain regions in the US and China. However, the RF-regional  
366 method does not outperform all the other approaches in every location despite its better overall performance (see figures A14  
367 and A15). This suggests that using multiple statistical approaches may be necessary to derive robust conclusions for attributing  
368 pollutant trends to emission changes.

369 With our model experiments, we also quantify the estimation errors in assuming emission impacts can be perfectly separated  
370 from meteorological variability. These errors likely bound the estimation errors that can be achieved by any statistical methods  
371 with this assumption. In the future, more complex statistical and machine learning methods could be applied to distinguish  
372 emissions- and meteorologically-driven changes, but attribution solely based on observed concentrations and meteorology will  
373 be limited by physical interactions between emissions and meteorology. We find that the estimation errors resulting from these  
374 interactions are overall much smaller compared to the estimation errors of the existing statistical methods, but can still be  
375 important for certain regions at certain times. However, the intertwined relationships between anthropogenic emissions and  
376 meteorology are often much more complex in reality compared to our model experiments. For example, meteorology can also  
377 directly influence anthropogenic emissions (e.g., increased electricity consumption during extreme weather conditions (U.S.  
378 Energy Information Agency, 2019; He et al., 2020)). Therefore, the estimation errors that can be achieved by more flexible  
379 statistical models can potentially be even larger than the errors quantified with our constant-emis approach.

380 While the GEOS-Chem model provides us with a framework to test statistical methods, its use in our model experiments  
381 introduces some uncertainty and limitations. Specifically, our experiments assess the performance of statistical methods in cor-  
382 recting for the meteorology-pollution relationships encoded in GEOS-Chem, which may differ from the complex relationships  
383 in the observational data. Several studies have shown that GEOS-Chem and similar models do not capture certain meteorology-  
384 pollution relationships in the observational data (e.g., temperature -  $O_3$  relationship (Porter and Heald (2019)) and influence  
385 of regional meteorological patterns (Fiore et al. (2009))). The relationships encoded in GEOS-Chem may be different from

386 the underlying meteorology-pollution relationships in the following three ways: (1) parameters in GEOS-Chem that describe  
387 these relationships are uncertain; (2) the relationships in GEOS-Chem are incorrect or incomplete; and (3) the relationships  
388 in GEOS-Chem are deterministic compared to the potential stochastic underlying processes. Therefore, the performance of  
389 any individual statistical method is likely to be worse in the real world compared to its ability to reproduce a deterministic  
390 meteorology-pollution relationship encoded in GEOS-Chem. Further model-based experiments could apply our methods to  
391 different atmospheric models in order to test if these conclusions differ by different models.

392 Changes in natural emissions due to meteorological variability play an important role in the air quality-meteorology relation-  
393 ship. Our model experiment considers natural emission changes that can be simulated online with assimilated meteorological  
394 fields in GEOS-Chem, including soil  $\text{NO}_x$  emissions, biogenic VOC emissions, and dust emissions. We find that the statis-  
395 tical models perform notably worse in correcting for the variability in dust-related  $\text{PM}_{2.5}$  (see figure A12 for results using  
396 RF-regional), likely because dust  $\text{PM}_{2.5}$  is extremely variable, with zero concentration on most non-dust days but extremely  
397 high concentration during the occasional dust storms. Our findings can potentially shed light on another important source of  
398 natural emissions, wildfire emissions, which are also quite variable but have become an increasingly important contributor  
399 to  $\text{PM}_{2.5}$  and  $\text{O}_3$  in certain regions (e.g., western US) (Burke et al., 2021). While emissions from biomass burning are held  
400 constant in our model experiments as the wildfire emissions are prescribed in GEOS-Chem, wildfire emissions are significantly  
401 influenced by climatic variability (Abatzoglou and Williams, 2016; Xie et al., 2022) and will likely be a substantial challenge  
402 for any meteorological correction method in the future that attempts to separate changes in anthropogenic emissions from the  
403 variability in climate and associated natural emissions.

404 Our research reveals multiple directions for future research to enhance our understanding of the usage of statistical models  
405 to evaluate trends in pollutant concentrations under changing meteorological conditions. One key but challenging question  
406 is to better understand the estimation errors of these existing approaches, e.g. why the MLR model is able to correct for the  
407 meteorological variability in some locations but not others. In this paper, we only test a selection of methods based on their  
408 popularity in the existing literature and propose a simple-to-use model (RF-regional). More complex models (such as convo-  
409 lutional neural networks) may offer better performance, but the estimation error will likely be bounded by the errors of the  
410 constant-emis approach. Our work only evaluates the statistical and machine learning models in expressions 1 and 2, which  
411 only represent one (popular) set of evaluations that performs location-specific trend estimation with adjustments for meteo-  
412 rology and secular trends. However, other statistical model specifications specifically targeted to questions of meteorological  
413 interaction or that permit borrowing information across locations may generate different results. Constrained by computational  
414 resources and availability of emission inventories, our simulation only covers a relatively short time period which could result  
415 in additional uncertainty in the linear trend estimates. When possible, future studies could evaluate performances of the statisti-

416 cal models with longer simulations and alternative trend estimates (such as the Theil-Sen estimator). A deeper investigation of  
417 the estimation error due to assuming perfect separation between meteorology and emission is also essential for understanding  
418 how we should interpret studies that use these statistical methods. For example, further work could explore how these errors  
419 will vary by the magnitude of emissions reductions and the chemistry regimes.

## 420 **5 Recommendations for attributing trends to emissions changes**

421 Using statistical methods to causally infer relationships between simulated air pollutant concentrations and anthropogenic  
422 emissions is challenging, and doing so in contexts of observational data is even more challenging. Understanding the uncer-  
423 tainty of statistical models in characterizing the meteorology-pollution relationship is essential to evaluating the effectiveness  
424 of policy interventions with observational data. Here, we make several recommendations to researchers and policy makers  
425 based on our analysis.

426 For those who aim to infer causal effects of emissions changes on air quality based on observational data on concentrations  
427 and meteorology, we recommend using multiple statistical methods to correct for meteorological variability when evaluating  
428 the impacts of policies or interventions on air quality. From our two case studies, we find a relatively large variation between the  
429 trend parameters estimated by different statistical methods (especially at the grid cell or monitor level). Some methods perform  
430 better in certain locations but not in others (though RF-regional is the best-performing method overall). Using multiple ap-  
431 proaches (linear/non-linear and at local/regional scale) may help to quantify uncertainty related to meteorological corrections.  
432 These findings also suggest that empirical analyses may benefit from considering the impacts of meteorological variability on  
433 air quality separately for each region or even for each monitor location (if data permits), instead of attempting to determine a  
434 general relationship between meteorological variability and air pollution over a large spatial domain. Finally, analysts should  
435 be particularly cautious when using statistical methods to estimate impacts of anthropogenic emissions on air quality in regions  
436 where pollution variability is dominated by meteorologically-influenced environmental processes such as dust emissions, as  
437 we consistently show that typical statistical methods (in combination with the standard set of meteorological variables) do not  
438 work well in those regions.

439 Due to the non-negligible estimation errors in recovering the counterfactual trends even with the best-performing statistical  
440 approach we test, we believe these statistical analyses are most useful in understanding the patterns of anthropogenic emissions  
441 on air quality when aggregated across larger spatial areas, rather than providing specific trends for individual monitor locations.  
442 There is a higher degree of consistency among the trend estimates across different methods when aggregated at regional level,  
443 but assessment at local level is more sensitive to method choice. The absolute magnitude of monitor-level trends needs to be

444 interpreted with caution, considering both the uncertainty from the statistical methods and also the limit of meteorological  
445 correction due to ignoring the interactions between meteorology and emissions.

446 Because measured pollutant concentrations are subject to the influence of underlying meteorological variability, many efforts  
447 have attempted to correct for the impacts of meteorological variability and use “meteorology-corrected” concentrations and  
448 trends to assist in evaluating the effectiveness of air quality policies. Our study evaluates existing methods that aim to correct for  
449 the meteorological variability and finds many of these methods do not perform well. This raises potential concerns about the use  
450 of “meteorology-corrected” concentrations as targets for policy evaluation. Meteorology-corrected concentrations and trends  
451 remain useful metrics to quantify the influence of emissions. However, a more comprehensive evaluation of the effectiveness  
452 of policy requires interpreting measurements with all available tools, ideally including both statistical analyses and physical  
453 models.

454 *Code and data availability.* The GEOS-Chem simulation of different scenarios and the R scripts to implement the statistical methods to  
455 correct for meteorological variability are available at the following repository: <https://doi.org/10.5281/zenodo.6857259>. All the other data  
456 needed to evaluate the conclusions in the paper are present in the paper.

457 *Author contributions.* M.Q. and N.E.S. designed the research. M.Q. performed the statistical analysis and GEOS-Chem modeling simula-  
458 tions. All authors interpreted the results and wrote the paper.

459 *Competing interests.* The authors declare no competing interests.

460 *Acknowledgements.* We thank Colette Heald and Valerie Karplus for helpful comments and discussions. We thank Yixuan Zheng for assis-  
461 tance with the MEIC emissions inventory. We thank Ke Li for sharing code of step-wise MLR analysis. This publication was supported by  
462 US EPA grant RD-835872-01. Its contents are solely the responsibility of the grantee and do not necessarily represent the official views of  
463 the USEPA. Further, USEPA does not endorse the purchase of any commercial products or services mentioned in the publication. This work  
464 was also supported by NIH grant NIEHS R01ES026217. M.Q. gratefully acknowledges the support from the MIT Martin Family Society of  
465 Fellows for Sustainability.

## 466 References

- 467 Abatzoglou, J. T. and Williams, A. P.: Impact of anthropogenic climate change on wildfire across western US forests, Proceedings of the  
468 National Academy of Sciences, 113, 11 770–11 775, 2016.
- 469 Beijing Municipal Ecology and Environment Bureau: Beijing Clean Air Action Plan (2013–2017), 744, 140 837, [http://sthjj.beijing.gov.cn/  
470 bjhrb/index/xxgk69/sthjlyzgw/wrygl/603133/index.html](http://sthjj.beijing.gov.cn/bjhrb/index/xxgk69/sthjlyzgw/wrygl/603133/index.html), 2013.
- 471 Bey, I., Jacob, D. J., Yantosca, R. M., Logan, J. A., Field, B. D., Fiore, A. M., Li, Q., Liu, H. Y., Mickley, L. J., and Schultz, M. G.: Global  
472 modeling of tropospheric chemistry with assimilated meteorology: Model description and evaluation, Journal of Geophysical Research  
473 Atmospheres, 106, 23 073–23 095, <https://doi.org/10.1029/2001JD000807>, 2001.
- 474 Burke, M., Driscoll, A., Heft-Neal, S., Xue, J., Burney, J., and Wara, M.: The changing risk and burden of wildfire in the United States,  
475 Proceedings of the National Academy of Sciences, 118, 2021.
- 476 Camalier, L., Cox, W., and Dolwick, P.: The effects of meteorology on ozone in urban areas and their use in assessing ozone trends, Atmo-  
477 spheric Environment, 41, 7127–7137, <https://doi.org/10.1016/j.atmosenv.2007.04.061>, 2007.
- 478 Carslaw, D. C., Beevers, S. D., and Tate, J. E.: Modelling and assessing trends in traffic-related emissions using a generalised additive  
479 modelling approach, Atmospheric Environment, 41, 5289–5299, <https://doi.org/10.1016/j.atmosenv.2007.02.032>, 2007.
- 480 Chen, L., Zhu, J., Liao, H., Yang, Y., and Yue, X.: Meteorological influences on PM<sub>2.5</sub> and O<sub>3</sub> trends and associated health burden since  
481 China’s clean air actions, Science of The Total Environment, 744, 140 837, 2020.
- 482 Chen, Z., Chen, D., Kwan, M. P., Chen, B., Gao, B., Zhuang, Y., Li, R., and Xu, B.: The control of anthropogenic emissions contributed  
483 to 80% of the decrease in PM<sub>2.5</sub> concentrations in Beijing from 2013 to 2017, Atmospheric Chemistry and Physics, 19, 13 519–13 533,  
484 <https://doi.org/10.5194/acp-19-13519-2019>, 2019.
- 485 Cheng, J., Su, J., Cui, T., Li, X., Dong, X., Sun, F., Yang, Y., Tong, D., Zheng, Y., Li, Y., Li, J., Zhang, Q., and He, K.: Dominant role of  
486 emission reduction in PM<sub>2.5</sub> air quality improvement in Beijing during 2013–2017: A model-based decomposition analysis, Atmospheric  
487 Chemistry and Physics, 19, 6125–6146, <https://doi.org/10.5194/acp-19-6125-2019>, 2019.
- 488 Chernozhukov, V., Chetverikov, D., Demirer, M., Duflo, E., Hansen, C., Newey, W., and Robins, J.: Double/debiased machine learning for  
489 treatment and structural parameters, 2018.
- 490 China’s Ministry of Ecology and Environment: National Air Quality Monitoring Data, <https://quotsoft.net/air/>, 2021.
- 491 European Union: Air Quality Standards in the European Union, 744, 140 837, <https://ec.europa.eu/environment/air/quality/standards.htm>,  
492 2020.
- 493 Fiore, A. M., Dentener, F., Wild, O., Cuvelier, C., Schultz, M., Hess, P., Textor, C., Schulz, M., Doherty, R., Horowitz, L., et al.: Multimodel  
494 estimates of intercontinental source-receptor relationships for ozone pollution, Journal of Geophysical Research: Atmospheres, 114, 2009.
- 495 Gelaro, R., McCarty, W., Suárez, M. J., Todling, R., Molod, A., Takacs, L., Randles, C. A., Darmenov, A., Bosilovich, M. G., Reichle, R.,  
496 et al.: The modern-era retrospective analysis for research and applications, version 2 (MERRA-2), Journal of climate, 30, 5419–5454,  
497 2017.



498 Grange, S. K., Carslaw, D. C., Lewis, A. C., Boleti, E., and Hueglin, C.: Random forest meteorological normalisation models for Swiss  
499 PM10 trend analysis, *Atmospheric Chemistry and Physics*, 18, 6223–6239, <https://doi.org/10.5194/acp-18-6223-2018>, 2018.

500 Han, H., Liu, J., Shu, L., Wang, T., and Yuan, H.: Local and synoptic meteorological influences on daily variability in summertime surface  
501 ozone in eastern China, *Atmospheric Chemistry and Physics*, 20, 203–222, <https://doi.org/10.5194/acp-20-203-2020>, 2020.

502 Hayn, M., Beirle, S., Hamprecht, F. A., Platt, U., Menze, B. H., and Wagner, T.: Analysing spatio-temporal patterns of the global NO<sub>2</sub>-  
503 distribution retrieved from GOME satellite observations using a generalized additive model, *Atmospheric Chemistry and Physics*, 9,  
504 6459–6477, <https://doi.org/10.5194/acp-9-6459-2009>, 2009.

505 He, P., Liang, J., Qiu, Y. L., Li, Q., and Xing, B.: Increase in domestic electricity consumption from particulate air pollution, *Nature Energy*,  
506 5, 985–995, 2020.

507 Heald, C. L., Collett, J. L., Lee, T., Benedict, K. B., Schwandner, F. M., Li, Y., Clarisse, L., Hurtmans, D. R., Van Damme, M., Clerbaux, C.,  
508 Coheur, P. F., Philip, S., Martin, R. V., and Pye, H. O.: Atmospheric ammonia and particulate inorganic nitrogen over the United States,  
509 *Atmospheric Chemistry and Physics*, 12, 10295–10312, <https://doi.org/10.5194/acp-12-10295-2012>, 2012.

510 Henneman, L. R., Holmes, H. A., Mulholland, J. A., and Russell, A. G.: Meteorological detrending of primary and secondary pollutant  
511 concentrations: Method application and evaluation using long-term (2000–2012) data in Atlanta, *Atmospheric Environment*, 119, 201–  
512 210, <https://doi.org/10.1016/j.atmosenv.2015.08.007>, 2015.

513 Holland, D. M., Principe, P. P., and Sickles, J. E.: Trends in atmospheric sulfur and nitrogen species in the eastern United States for 1989–  
514 1995, *Atmospheric Environment*, 33, 37–49, [https://doi.org/10.1016/S1352-2310\(98\)00123-X](https://doi.org/10.1016/S1352-2310(98)00123-X), 1998.

515 Keller, C. A., Long, M. S., Yantosca, R. M., Da Silva, A., Pawson, S., and Jacob, D. J.: HEMCO v1. 0: a versatile, ESMF-compliant  
516 component for calculating emissions in atmospheric models, *Geoscientific Model Development*, 7, 1409–1417, 2014.

517 Leung, D. M., Tai, A. P., Mickley, L. J., Moch, J. M., Van Donkelaar, A., Shen, L., and Martin, R. V.: Synoptic meteorological modes of  
518 variability for fine particulate matter (PM<sub>2.5</sub>) air quality in major metropolitan regions of China, *Atmospheric Chemistry and Physics*, 18,  
519 6733–6748, <https://doi.org/10.5194/acp-18-6733-2018>, 2018.

520 Li, C., Martin, R. V., Van Donkelaar, A., Boys, B. L., Hammer, M. S., Xu, J. W., Marais, E. A., Reff, A., Strum, M., Ridley, D. A., Crippa,  
521 M., Brauer, M., and Zhang, Q.: Trends in Chemical Composition of Global and Regional Population-Weighted Fine Particulate Matter  
522 Estimated for 25 Years, *Environmental Science and Technology*, 51, 11185–11195, <https://doi.org/10.1021/acs.est.7b02530>, 2017a.

523 Li, K., Jacob, D. J., Liao, H., Shen, L., Zhang, Q., and Bates, K. H.: Anthropogenic drivers of 2013–2017 trends in summer  
524 surface ozone in China., *Proceedings of the National Academy of Sciences of the United States of America*, 116, 422–427,  
525 <https://doi.org/10.1073/pnas.1812168116>, 2018.

526 Li, K., Jacob, D. J., Shen, L., Lu, X., De Smedt, I., and Liao, H.: Increases in surface ozone pollution in China from 2013 to 2019: anthro-  
527 pogenic and meteorological influences, *Atmospheric Chemistry and Physics*, 20, 11423–11433, 2020.

528 Li, M., Liu, H., Geng, G., Hong, C., Liu, F., Song, Y., Tong, D., Zheng, B., Cui, H., Man, H., Zhang, Q., and He, K.: Anthropogenic emission  
529 inventories in China: A review, *National Science Review*, 4, 834–866, <https://doi.org/10.1093/nsr/nwx150>, 2017b.

530 Lu, X., Zhang, L., Chen, Y., Zhou, M., Zheng, B., Li, K., Liu, Y., Lin, J., Fu, T. M., and Zhang, Q.: Exploring 2016-2017 surface  
531 ozone pollution over China: Source contributions and meteorological influences, *Atmospheric Chemistry and Physics*, 19, 8339–8361,  
532 <https://doi.org/10.5194/acp-19-8339-2019>, 2019.

533 Lu, X., Zhang, L., Wang, X., Gao, M., Li, K., Zhang, Y., Yue, X., and Zhang, Y.: Rapid increases in warm-season surface ozone and resulting  
534 health impact in China since 2013, *Environmental Science & Technology Letters*, 7, 240–247, 2020.

535 Ma, Z., Xu, J., Quan, W., Zhang, Z., Lin, W., and Xu, X.: Significant increase of surface ozone at a rural site, north of eastern China,  
536 *Atmospheric Chemistry and Physics*, 16, 3969–3977, <https://doi.org/10.5194/acp-16-3969-2016>, 2016.

537 McClure, C. D. and Jaffe, D. A.: US particulate matter air quality improves except in wildfire-prone areas, *Proceedings of the National  
538 Academy of Sciences of the United States of America*, 115, 7901–7906, <https://doi.org/10.1073/pnas.1804353115>, 2018.

539 Otero, N., Sillmann, J., Mar, K. A., Rust, H. W., Solberg, S., Andersson, C., Engardt, M., Bergström, R., Bessagnet, B., Colette, A., Couvidat,  
540 F., Cuvelier, C., Tsyro, S., Fagerli, H., Schaap, M., Manders, A., Mircea, M., Briganti, G., Cappelletti, A., Adani, M., D’Isidoro, M., Pay,  
541 M. T., Theobald, M., Vivanco, M. G., Wind, P., Ojha, N., Raffort, V., and Butler, T.: A multi-model comparison of meteorological drivers  
542 of surface ozone over Europe, *Atmospheric Chemistry and Physics*, 18, 12 269–12 288, <https://doi.org/10.5194/acp-18-12269-2018>, 2018.

543 Porter, W. C. and Heald, C. L.: The mechanisms and meteorological drivers of the ozone–temperature relationship, *Atmospheric Chemistry  
544 and Physics Discussions*, pp. 1–26, <https://doi.org/10.5194/acp-2019-140>, 2019.

545 Qu, L., Liu, S., Ma, L., Zhang, Z., Du, J., Zhou, Y., and Meng, F.: Evaluating the meteorological normalized PM2.5 trend  
546 (2014–2019) in the “2+26” region of China using an ensemble learning technique, *Environmental Pollution*, 266, 115 346,  
547 <https://doi.org/10.1016/j.envpol.2020.115346>, 2020.

548 Runge, J., Bathiany, S., Bollt, E., Camps-Valls, G., Coumou, D., Deyle, E., Glymour, C., Kretschmer, M., Mahecha, M. D., Muñoz-Marí, J.,  
549 van Nes, E. H., Peters, J., Quax, R., Reichstein, M., Scheffer, M., Schölkopf, B., Spirtes, P., Sugihara, G., Sun, J., Zhang, K., and Zscheis-  
550 chler, J.: Inferring causation from time series in Earth system sciences, *Nature Communications*, 10, 1–13, [https://doi.org/10.1038/s41467-  
551 019-10105-3](https://doi.org/10.1038/s41467-019-10105-3), 2019.

552 Saari, R., Mei, Y., Monier, E., and Garcia-Menendez, F.: Effect of Health-related Uncertainty and Natural Variability on Health Impacts and  
553 Co-Benefits of Climate Policy, *Environmental Science and Technology*, 53, 1098–1108, <https://doi.org/10.1021/acs.est.8b05094>, 2019.

554 Shen, L., Mickley, L. J., and Tai, A. P.: Influence of synoptic patterns on surface ozone variability over the eastern United States from 1980  
555 to 2012, *Atmospheric Chemistry and Physics*, 15, 10 925–10 938, <https://doi.org/10.5194/acp-15-10925-2015>, 2015.

556 Sherwen, T., Schmidt, J. A., Evans, M. J., Carpenter, L. J., Großmann, K., Eastham, S. D., Jacob, D. J., Dix, B., Koenig, T. K., Sinreich, R., Or-  
557 tega, I., Volkamer, R., Saiz-Lopez, A., Prados-Roman, C., Mahajan, A. S., and Ordóñez, C.: Global impacts of tropospheric halogens (Cl,  
558 Br, I) on oxidants and composition in GEOS-Chem, *Atmospheric Chemistry and Physics*, 16, 12 239–12 271, [https://doi.org/10.5194/acp-  
559 16-12239-2016](https://doi.org/10.5194/acp-16-12239-2016), 2016.

560 Shi, Z., Song, C., Liu, B., Lu, G., Xu, J., Van Vu, T., Elliott, R. J., Li, W., Bloss, W. J., and Harrison, R. M.: Abrupt but smaller than expected  
561 changes in surface air quality attributable to COVID-19 lockdowns, *Science Advances*, 7, <https://doi.org/10.1126/sciadv.abd6696>, 2021.

562 State Council of the People's Republic of China: The Air Pollution Prevention and Control Action Plan (2013–2017), 744, 140 837, [http://www.gov.cn/zw/gk/2013-09/12/content\\_2486773.htm](http://www.gov.cn/zw/gk/2013-09/12/content_2486773.htm), 2013.

564 Tai, A. P., Mickley, L. J., Jacob, D. J., Leibensperger, E. M., Zhang, L., Fisher, J. A., and Pye, H. O.: Meteorological modes of variability  
565 for fine particulate matter (PM<sub>2.5</sub>) air quality in the United States: Implications for PM<sub>2.5</sub> sensitivity to climate change, *Atmospheric  
566 Chemistry and Physics*, 12, 3131–3145, <https://doi.org/10.5194/acp-12-3131-2012>, 2012.

567 Tian, R., Ma, X., and Zhao, J.: A revised mineral dust emission scheme in GEOS-Chem: Improvements in dust simulations over China,  
568 *Atmospheric Chemistry and Physics*, 21, 4319–4337, <https://doi.org/10.5194/acp-21-4319-2021>, 2021.

569 Travis, K. R., Jacob, D. J., Fisher, J. A., Kim, P. S., Marais, E. A., Zhu, L., Yu, K., Miller, C. C., Yantosca, R. M., Sulprizio, M. P., Thompson,  
570 A. M., Wennberg, P. O., Crouse, J. D., St Clair, J. M., Cohen, R. C., Laughner, J. L., Dibb, J. E., Hall, S. R., Ullmann, K., Wolfe, G. M.,  
571 Pollack, I. B., Peischl, J., Neuman, J. A., and Zhou, X.: Why do models overestimate surface ozone in the Southeast United States?,  
572 *Atmospheric Chemistry and Physics*, 16, 13 561–13 577, <https://doi.org/10.5194/acp-16-13561-2016>, 2016.

573 U.S. Energy Information Agency: Heat wave results in highest U.S. electricity demand since 2017, 744, 140 837, [https://www.eia.gov/  
574 todayinenergy/detail.php?id=40253](https://www.eia.gov/todayinenergy/detail.php?id=40253), 2019.

575 U.S. Environmental Protection Agency: NATIONAL PRIMARY AND SECONDARY AMBIENT AIR QUALITY STANDARDS, 744,  
576 140 837, <https://ecfr.federalregister.gov/current/title-40/chapter-I/subchapter-C/part-50>, 2019.

577 U.S. Environmental Protection Agency: Criteria pollutants National Tier 1 for 1970 - 2020, 744, 140 837, [https://www.epa.gov/  
578 air-emissions-inventories/air-pollutant-emissions-trends-data](https://www.epa.gov/air-emissions-inventories/air-pollutant-emissions-trends-data), 2021a.

579 U.S. Environmental Protection Agency: Air Data: Air Quality Data Collected at Outdoor Monitors Across the US, [https://aqs.epa.gov/  
580 aqsweb/airdata/download\\_files.html#Meta/](https://aqs.epa.gov/aqsweb/airdata/download_files.html#Meta/), 2021b.

581 Vu, T., Shi, Z., Cheng, J., Zhang, Q., He, K., Wang, S., and Harrison, R.: Assessing the impact of Clean Air Action Plan on Air Quality Trends  
582 in Beijing Megacity using a machine learning technique, *Atmospheric Chemistry and Physics*, pp. 1–18, [https://doi.org/10.5194/acp-2019-  
583 173](https://doi.org/10.5194/acp-2019-173), 2019.

584 Wang, Y. X., McElroy, M. B., Jacob, D. J., and Yantosca, R. M.: A nested grid formulation for chemical transport over Asia: Applications to  
585 CO, *Journal of Geophysical Research: Atmospheres*, 109, <https://doi.org/10.1029/2004JD005237>, 2004.

586 Wells, B., Dolwick, P., Eder, B., Evangelista, M., Foley, K., Mannshardt, E., Misenis, C., and Weishampel, A.: Improved estimation of trends  
587 in US ozone concentrations adjusted for interannual variability in meteorological conditions, *Atmospheric Environment*, 248, 118 234,  
588 2021.

589 Werf, G. R., Randerson, J. T., Giglio, L., Leeuwen, T. T. v., Chen, Y., Rogers, B. M., Mu, M., Van Marle, M. J., Morton, D. C., Collatz, G. J.,  
590 et al.: Global fire emissions estimates during 1997–2016, *Earth System Science Data*, 9, 697–720, 2017.

591 Wood, S. N.: Fast stable restricted maximum likelihood and marginal likelihood estimation of semiparametric generalized linear models,  
592 *Journal of the Royal Statistical Society (B)*, 73, 3–36, 2011.

593 Xie, Y., Wang, Y., Dong, W., Wright, J. S., Shen, L., and Zhao, Z.: Evaluating the Response of Summertime Surface Sulfate to Hydroclimate  
594 Variations in the Continental United States: Role of Meteorological Inputs in the GEOS-Chem Model, *Journal of Geophysical Research:*  
595 *Atmospheres*, 124, 1662–1679, <https://doi.org/10.1029/2018JD029693>, 2019.

596 Xie, Y., Lin, M., Decharme, B., Delire, C., Horowitz, L. W., Lawrence, D. M., Li, F., and Séférian, R.: Tripling of western US particulate  
597 pollution from wildfires in a warming climate, *Proceedings of the National Academy of Sciences*, 119, e2111372 119, 2022.

598 Zhai, S., Jacob, D. J., Wang, X., Shen, L., Li, K., Zhang, Y., Gui, K., Zhao, T., and Liao, H.: Fine particulate matter (PM 2.5) trends in  
599 China, 2013–2018: Separating contributions from anthropogenic emissions and meteorology, *Atmospheric Chemistry and Physics*, 19,  
600 11 031–11 041, 2019.

601 Zhai, S., Jacob, D. J., Wang, X., Liu, Z., Wen, T., Shah, V., Li, K., Moch, J. M., Bates, K. H., Song, S., Shen, L., Zhang, Y., Luo, G., Yu, F.,  
602 Sun, Y., Wang, L., Qi, M., Tao, J., Gui, K., Xu, H., Zhang, Q., Zhao, T., Wang, Y., Lee, H. C., Choi, H., and Liao, H.: Control of particulate  
603 nitrate air pollution in China, *Nature Geoscience*, 14, 389–395, <https://doi.org/10.1038/s41561-021-00726-z>, 2021.

604 Zhang, H., Yuan, H., Liu, X., Yu, J., and Jiao, Y.: Impact of synoptic weather patterns on 24h-average PM2.5 concentrations in the North  
605 China Plain during 2013–2017, *Science of the Total Environment*, 627, 200–210, <https://doi.org/10.1016/j.scitotenv.2018.01.248>, 2018.

606 Zhang, Q., Zheng, Y., Tong, D., Shao, M., Wang, S., Zhang, Y., Xu, X., Wang, J., He, H., Liu, W., Ding, Y., Lei, Y., Li, J., Wang, Z., Zhang,  
607 X., Wang, Y., Cheng, J., Liu, Y., Shi, Q., Yan, L., Geng, G., Hong, C., Li, M., Liu, F., Zheng, B., Cao, J., Ding, A., Gao, J., Fu, Q., Huo,  
608 J., Liu, B., Liu, Z., Yang, F., He, K., and Hao, J.: Drivers of improved PM2.5 air quality in China from 2013 to 2017, *Proceedings of the*  
609 *National Academy of Sciences of the United States of America*, pp. 1–7, <https://doi.org/10.1073/pnas.1907956116>, 2019.

610 Zhang, Y., Vu, T. V., Sun, J., He, J., Shen, X., Lin, W., Zhang, X., Zhong, J., Gao, W., Wang, Y., Fu, T. M., Ma, Y., Li, W., and Shi, Z.:  
611 Significant Changes in Chemistry of Fine Particles in Wintertime Beijing from 2007 to 2017: Impact of Clean Air Actions, *Environmental*  
612 *Science and Technology*, 54, 1344–1352, <https://doi.org/10.1021/acs.est.9b04678>, 2020.

613 Zhao, Y., Zhang, K., Xu, X., Shen, H., Zhu, X., Zhang, Y., Hu, Y., and Shen, G.: Substantial Changes in Nitrate Oxide and Ozone after  
614 Excluding Meteorological Impacts during the COVID-19 Outbreak in Mainland China, *Environmental Science Technology Letters*,  
615 <https://doi.org/10.1021/acs.estlett.0c00304>, 2020.

616 Zheng, B., Tong, D., Li, M., Liu, F., Hong, C., Geng, G., Li, H., Li, X., Peng, L., Qi, J., et al.: Trends in China’s anthropogenic emissions  
617 since 2010 as the consequence of clean air actions, *Atmospheric Chemistry and Physics*, 18, 14 095–14 111, 2018.

618 Zhong, Q., Ma, J., Shen, G., Shen, H., Zhu, X., Yun, X., Meng, W., Cheng, H., Liu, J., Li, B., Wang, X., Zeng, E. Y., Guan, D., and Tao, S.:  
619 Distinguishing Emission-Associated Ambient Air PM2.5 Concentrations and Meteorological Factor-Induced Fluctuations, *Environmental*  
620 *Science and Technology*, 52, 10 416–10 425, <https://doi.org/10.1021/acs.est.8b02685>, 2018.

621 Zurbenko, I. G.: Detecting and tracking changes in ozone air quality, *Air and Waste*, 44, 1089–1092,  
622 <https://doi.org/10.1080/10473289.1994.10467303>, 1994.